Biosensors and Bioelectronics 145 (2019) 111729

Contents lists available at ScienceDirect

Biosensors and Bioelectronics

journal homepage: http://www.elsevier.com/locate/bios

Orthogonal dual molecularly imprinted polymer-based plasmonic immunosandwich assay: A double characteristic recognition strategy for specific detection of glycoproteins

Lingli Zhou [a,1], Yijia Wang [a,1], Rongrong Xing [a], Jin Chen [b], Jia Liu [a], Wei Li [a], Zhen Liu [a,*]

[a] State Key Laboratory of Analytical Chemistry for Life Science, School of Chemistry and Chemical Engineering, Nanjing University, Nanjing, 210023, China
[b] Department of Medical Oncology, Jiangsu Cancer Hospital, Nanjing, 210009, China

ARTICLE INFO

Keywords:
Molecularly imprinted polymer
Glycoprotein
Plasmonic immunosandwich assay
Glycosylation
Epitope
Raman spectroscopy

ABSTRACT

Sensitive and specific detection methods are critical to the detection of glycoproteins. Immunoassay has been a powerful tool for this purpose, in which antibodies or their mimics particularly molecularly imprinted polymers (MIPs) are used for specific recognition. Epitope and glycan are two structure features of a glycoprotein. However, immunoassays based on simultaneous recognition towards the two characteristics have been scarcely explored so far. Herein we present a new strategy called orthogonal dual molecularly imprinted polymer-based plasmonic immunosandwich assay (odMIP-PISA). It relies on double recognition towards a target glycoprotein by two different types of MIPs, using epitope-imprinted gold nanoparticles (AuNPs)-coated slide as capturing substrate to recognize the peptide epitope and glycans-imprinted Raman-active silver nanoparticles as labeling nanotags to recognize the glycans. Carcinoembryonic antigen (CEA), a routinely used marker for colon cancer, was used as a test glycoprotein. The orthogonal double recognition apparently improved the specificity, reducing the maximum cross-reactivity from 14.4% for epitope recognition and 15.2% for glycan recognition to 8.2% for double recognition. Meanwhile, the plasmonic nanostructure-based Raman detection provided ultrahigh sensitivity, yielding a limit of detection of 5.56×10^{-14} M (S/N = 10). Through measuring the CEA level in human serum, this method permitted differentiation of colon cancer patient from healthy individual. Compared with the traditional immunoassay, odMIP-PISA exhibited multiple advantages, including simplified procedure (6 steps), speed (30 min), reduced cost, and so on. Therefore, this new approach holds great promise in many applications particularly clinical diagnosis.

1. Introduction

Glycosylation of proteins is the most common post-modification in organisms. In mammals, more than 50% of the proteins are glycoproteins. Glycoproteins play crucial roles in many important biological events such as cell adhesion, signaling, development, host-pathogen interactions, and immune responses (Li and Wang, 2018). Abnormal glycosylation often correlates closely with disease development and progression such as cancer, inflammation, and some congenital diseases (Lehle et al., 2006; Deshayes et al., 2013; Kammeijer et al., 2018). Thus, many glycoproteins, such as alpha fetoprotein (AFP) and carcinoembryonic antigen (CEA), have been routinely used as cancer markers (Kimura et al., 1996; Laboria et al., 2010). However, the detection of glycoproteins with important biological significance is often challenging. This is because that they are often present in very low concentration in biological samples, and meanwhile highly abundant interfering components are co-existing. Therefore, sensitive and specific detection methods are critical to the detection of trace glycoprotein biomarkers in clinical samples.

Immunoassay, particularly enzyme-linked immunosorbent assay (ELISA), has been an important tool for the detection of glycoprotein biomarkers in clinical diagnosis, in which highly specific antibodies are critical (Gervay and Mcreynolds, 1999; Bigalke et al., 2011; Yazawa et al., 2018; Engvall and Perlmann, 1971; Clark and Adams, 1977). However, the preparation of high-quality antibodies is tedious and costly. Besides, antibodies are associated with apparent disadvantages

* Corresponding author.
E-mail address: zhenliu@nju.edu.cn (Z. Liu).
[1] These authors contributed equally to this work.

https://doi.org/10.1016/j.bios.2019.111729
Received 31 July 2019; Received in revised form 20 September 2019; Accepted 21 September 2019
Available online 25 September 2019

such as poor stability and poor reproducibility (Baker, 2015a, 2015b). More importantly, due to the weak immunogenicity and poor availability, the preparation of glycan-specific antibodies is facing serious challenges (Sterner et al., 2016). Although lectins have been used as recognition reagents in immunoassay (Haab, 2010; Yue et al., 2009), their relatively poor specificity limits the applications. On the other hand, antibody mimics have also been used to construct new immunoassays. Aptamers, which are short single-stranded DNA or RNA or peptide with the ability to bind specific species, have been widely used as alternatives of one or two antibodies to create immunoassays (Qin et al., 2017; Yazdanparast et al., 2018; Zhou et al., 2016; Kim and Lee, 2015; Cho et al., 2019). However, aptamers recognizing the glycan structure of proteins are challenging to discover (Diaz-Fernandez et al., 2019). Besides, molecularly imprinted polymers (MIPs) (Wulff and Sarhan, 1972; Andersson et al., 1984; Vlatakis et al., 1993; Liu and Wulff, 2004; Nishino et al., 2006; Adbo and Nicholls, 2001; Kubo et al., 2006; Wang et al., 2009; Awino and Zhao, 2013; Li et al., 2013, 2014, 2019; Bie et al., 2015, 2018; Xing et al., 2017, 2019), which are artificial receptors synthesized through polymerization in the presence of the target, have been also used as antibody alternatives in immunoassay development (Surugiu et al., 2000; Smolinska-Kempisty et al., 2016; Xu et al., 2017; Bi and Liu, 2014; Chianella et al., 2013; Sun et al., 2019). Compared to antibodies, MIPs are more cost-efficient, easier to prepare, and more stable. By combining boronate affinity MIPs with surface-enhanced Raman scattering (SERS), which is an ultrasensitive detection method, we have developed two new antibody-free and enzyme-free approaches, including boronate affinity sandwich assay (BASA) (Ye et al., 2014) and plasmonic immunosandwich assay (PISA) (Tu et al., 2016). Both BASA and PISA have been successfully applied to the detection of glycoproteins in human serum (Muhammad et al., 2017; You et al., 2017; Usta et al., 2016) and urine (Tu et al., 2016). PISA was also a powerful tool for the determination of glycoproteins in single living cells or living animals (Liu et al., 2016). However, in both current BASA and PISA, only single MIPs have been used for target recognition.

Peptide epitope and glycan are two structure features of a glycoprotein. If an immunoassay is based on simultaneous recognitions towards these two characteristics, the specificity can be largely improved. However, as stated above, no matter in antibody-based or antibody mimic-based immunoassays, so far, few works have been based on simultaneous recognitions of the peptide epitope as well as the glycans of a target glycoprotein.

Herein, we present a new strategy called orthogonal dual molecularly imprinted polymer-based plasmonic immunosandwich assay (odMIP-PISA) for the specific detection of glycoproteins. This new strategy relies on double recognition by two different type of MIPs, one recognizing the epitope of the target glycoprotein while the other recognizing the glycans. Epitope is an accessible characteristic short peptide at the N-terminal or C-terminal of the polypeptide chain while glycans are characteristics of the post-translational modification (PTM) of a glycoprotein. Since epitope and glycans are different characteristics of the target molecule, their recognition by two MIPs generates an orthogonal double characteristic recognition, which can provide a double-check mechanism and thereby can be expected to be able to improve the overall recognition specificity as compared with single recognition. The principle and procedure of odMIP-PISA are illustrated in Scheme 1. An MIP thinlayer specific to the C- or N-terminal epitope of a target glycoprotein is prepared on an AuNPs self-assembled monolayer (SAM)-coated glass slide according to the boronate affinity-assisted oriented surface imprinting (Xing et al., 2019). The prepared epitope-imprinted slide is used as a target capturing substrate. On the other hand, glycans digested from the glycoprotein are purified as templates. Glycans-imprinted Raman-active Ag-cored nanoparticles (NPs) are prepared as Raman labeling nanotags. A drop of serum sample is pipetted on the epitope-imprinted slide. After extraction, unwanted species are washed away and then the captured glycoprotein is labeled with glycan-imprinted Raman nanotags. Thus, sandwich-like immunocomplexes are formed on the glass slide. After removing excessive Raman nanotags, the slide is subjected to Raman detection. Upon radiation with a laser beam, the Ag-cored Raman nanotags generate strong SERS signal. Meanwhile, due to plasmonic coupling, a hot spot is generated at the gap between the epitope-imprinted AuNPs SAM-coated slide and the Ag-cored Raman nanotags, which further enhances the SERS signal. As a proof of the principle, CEA, which has been routinely used as a marker for colon cancer, was used a test glycoprotein in this study. An epitope-imprinted extraction substrate and glycans-imprinted Raman nanotags that can recognize CEA from different aspects of structural characteristics were prepared. We demonstrated that the combined use of the two types of MIPs apparently improved the detection specificity. Facile detection of the CEA concentration in serum of a healthy individual and a colon cancer patient was achieved, which allowed for differentiation of the colon cancer patient from the healthy individual. Comparison of the odMIP-PISA method with ELISA based a commercial kit was made, which demonstrated several advantages of the current method over ELISA. Since glycan-specific antibodies are hard to prepared, the orthogonal double recognition-based assay holds unique strength over antibody-based immunoassays. As the imprinting

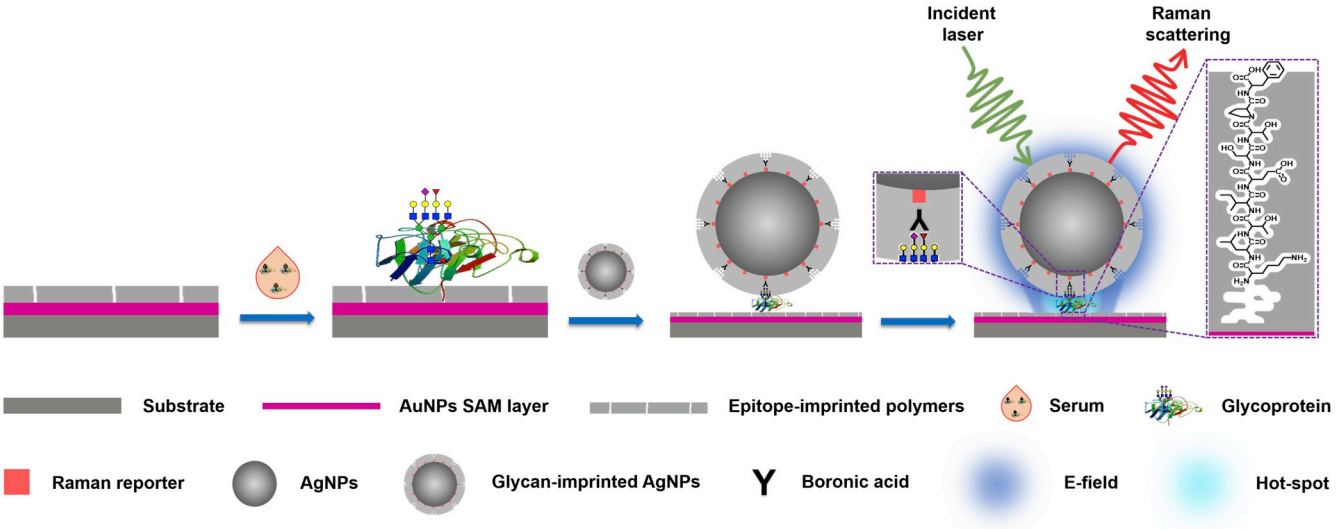

Scheme 1. Schematic illustration of odMIP-PISA approach for detection of trace target glycoprotein in complex sample.

approaches can be easily extended to other glycoprotein biomarkers, this new PISA approach can be a promising tool for clinical diagnosis.

2. Materials and methods

Details on experimental section are provided in the Supplementary Material.

3. Results and discussion

3.1. Synthesis and characterization

According to the amino acid sequence of CEA from the UniProt protein database, N-terminal nonapeptide (KLTIESTPF) was selected as the epitope peptide. In order to obtain glycated epitope as the imprinting template, a fructose was attached to the N-terminal lysine (K) moiety via the Maillard reaction. The structure of the N-terminal epitope and its glycation process are illustrated in Fig. S1 because the epitope peptide contains amino acids with different properties, four silylating reagents containing functionalities capable of interacting with the template, including aminopropyltriethoxysilane (APTES), 3-ureidopropyl-triethoxysilane (UPTES), isobutyltriethoxysilane (IBTES) and tetraethyl orthosilicate (TEOS) (Fig. S2) were selected as functional monomers for the synthesis of epitope-imprinted arrays. The synthesis route is illustrated in Fig. S3. On the other hand, glycan-imprinted SERS tags were prepared using the synthetic route described in Fig. S4.

The synthesized materials were characterized. From the data of dynamic light scattering (DLS) and transmission electronic microscopy (TEM) (Fig. S5A and Fig. S5B), the average diameters of AgNPs and glycan-imprinted Ag/p-mercaptonoaniline@SiO_2 NPs (Ag/PATP@SiO_2 NPs) were estimated to be 68 nm and 88 nm, respectively. This suggests that the silica shell of the glycan-imprinted Ag/PATP@SiO_2 NPs was approximately 10 nm in thickness. Both the TEM images and DLS data show that the nanoparticles exhibited good dispersibility and homogeneous size distribution. The extinction spectra for the nanoparticles at different steps of the preparation of the epitope-imprinted Ag/PATP@SiO_2 NPs were studied. As shown in Fig. S5C, Ag/PATP@SiO_2 NPs exhibited an obvious red-shift in the surface plasmon band of AgNPs, owing to the presence of a silica layer. After functionalization of Ag/PATP@SiO_2 NPs by 4-formylphenylboronic acid (FPBA), there was a blue shift. The obtained non-imprinted and glycan-imprinted Ag/PATP@SiO_2 NPs showed a red shift owing to the presence of the imprinting layer. At the same time, the extinction spectra of the non-imprinted and glycan-imprinted Ag/PATP@SiO_2 NPs were almost the same, which indicates that the non-imprinted Ag/PATP@SiO_2 NPs could be used as a comparison to evaluate the imprinting effect. The Raman spectra of AgNPs, Ag/PATP NPs, Ag/PATP@SiO_2 NPs, glycan-imprinted and non-imprinted Ag/PATP@SiO_2 NPs are shown in Fig. S5D. The Raman intensity of glycan-imprinted and non-imprinted Ag/PATP@SiO_2 NPs was slightly weaker than that of Ag/PATP NPs, indicating that they still had strong intensity as a SERS nanotag. It is noteworthy that the characteristic Raman peaks of glycan-imprinted Ag/PATP@SiO_2 NPs did not result from PATP, but its photocatalytic coupling reaction product 4,4-dimercaptoazobenzene (DMAB), generated on AgNPs by laser irradiation. According to the literature data (Y.F. Huang et al., 2010; Y.Z. Huang et al., 2010; Choi et al., 2013), the main Raman bands are assigned as follows: the peaks at 1,143, 1574 and 1073 cm^{-1} are assigned to the vibrational mode of C–N, C–C and C–S bonds, while peaks at 1435 and 1390 cm^{-1} are assigned to the N═N relative vibrational modes of DMAB. Herein, the characteristic peak at 1435 cm^{-1} was selected for quantitative detection. In addition, these nanoparticles were characterized by Fourier transform infrared spectroscopy (FT-IR) spectra, as shown in Fig. S5E. The absorption peaks at 1050 cm^{-1}, 1090 cm^{-1}, 1380 cm^{-1}, 1492 cm^{-1}, 1630 cm^{-1}, 2940 cm^{-1} and 3400 cm^{-1} are attributed to C–N, Si–O, C–H, C═C, C═O, C–H and N–H vibration, respectively. The appearance of 1492 cm^{-1} and 1090 cm^{-1} absorption peaks indicates that PATP was successfully modified and coated with silica. The appearance of 1050 cm^{-1} absorption peaks indicates that FPBA was successfully modified. The adsorption peak at 1090 cm^{-1} was enhanced, which suggests the formation of an imprinting layer on the nanoparticle surface. Moreover, the morphology and size of the synthesized AuNPs were characterized using TEM and DLS (Fig. S5F). The synthesized AuNPs exhibited spherical shape and a uniform size of ca. 60 nm. Finally, self-assembled monolayer (SAM) of AuNPs and epitope-imprinted AuNPs on a glass slide were characterized by scanning electronic microscopy (SEM), as shown in Figs. S5G and S5H. The well-formed SAM coating and uniformly dispersed size are highly favorable for the detection reproducibility as well as the detection sensitivity.

3.2. Optimization of monomer ratio and imprinting time for epitope imprinting

To obtain best binding properties, three different monomer compositions (which are selected in terms of the respective numbers of amino acids having different properties in the selected epitope with setting TEOS predominant to form a hydrophilic silica skeleton to reducing non-specific adsorption, see Table S1) as well as the imprinting time for each composition were optimized in terms of imprinting factor (IF). IF is defined as the ratio of the amount of template captured by the MIPs and non-imprinted polymers (NIPs) prepared under otherwise identical conditions. For the fructose-glycated epitope (Fru-KLTIESTPF), its length was estimated to be approximately 3.48 nm. According to the thickness-imprinting time dependence we established previously (Xing et al., 2019), imprinting time was set at 40, 50, 60, and 70 min. MIPs and NIPs prepared at each composition and each imprinting time were used to extract the target and captured target was eluted for UV absorbance detection. As shown in Fig. 1A, B and 1C, the best imprinting conditions was found to be composition B (ratio of APTES/UPTES/IBTES/TEOS: 15/15/30/40) and imprinting for 50 min, which gave the highest IF value of 4.83, which is comparable to the level for CEA imprinted hydrogel (Casey and Kofinas, 2010).

3.3. Optimization of imprinting time for glycan imprinting

As compared with above condition optimization for epitope imprinting, the condition optimization for glycan imprinting was simpler. The imprinting was performed according to the boronate affinity controllable oriented surface imprinting approach established previously (Bie et al., 2015; Xing et al., 2017), in which TEOS hydrolysis in ethanol was used to form an imprinting thin-layer on Ag/PATP@SiO_2 NPs while only the imprinting time was optimized. According to the protein database and related literature (Huang et al., 2015; Kannicht et al., 1999; Lucka et al., 2005), CEA has 28 N-linked glycosylation sites with more than 60 possible structurally different glycans (see Table S2). To be ideal Raman labeling tags, the glycan-imprinted Ag/PATP@SiO_2 NPs should be able to recognize most of the glycans if not all. According to the study previously published by our group (Bie et al., 2015), under exactly controlled conditions, the thickness of the silica layer increases linearly with increasing the imprinting time ($l = 0.51 + 0.04 \times t$, $R^2 = 0.994$, l is thickness in nm and t is imprinting time in min). To set a suitable range for imprinting time, several representative glycans with different lengths, including glycan A, glycan B, glycan C, glycan D and glycan E, were selected from the glycans shown in Table S2 and their estimated lengths via molecular simulation are shown in Table S3. According to the glycan lengths as well as above thickness-imprinting time linear relationship, the imprinting time was set within 50–80 min. Thus, four imprinting times, including 50, 60, 70, and 80 min, was investigated in terms of imprinting factor. As shown in Fig. 1D, the best imprinting time was found to be 60 min, which provided the highest IF value (12.3). Such IF value is much higher than that for imprinting of CEA (Casey and Kofinas, 2010). Under the optimal imprinting time, the

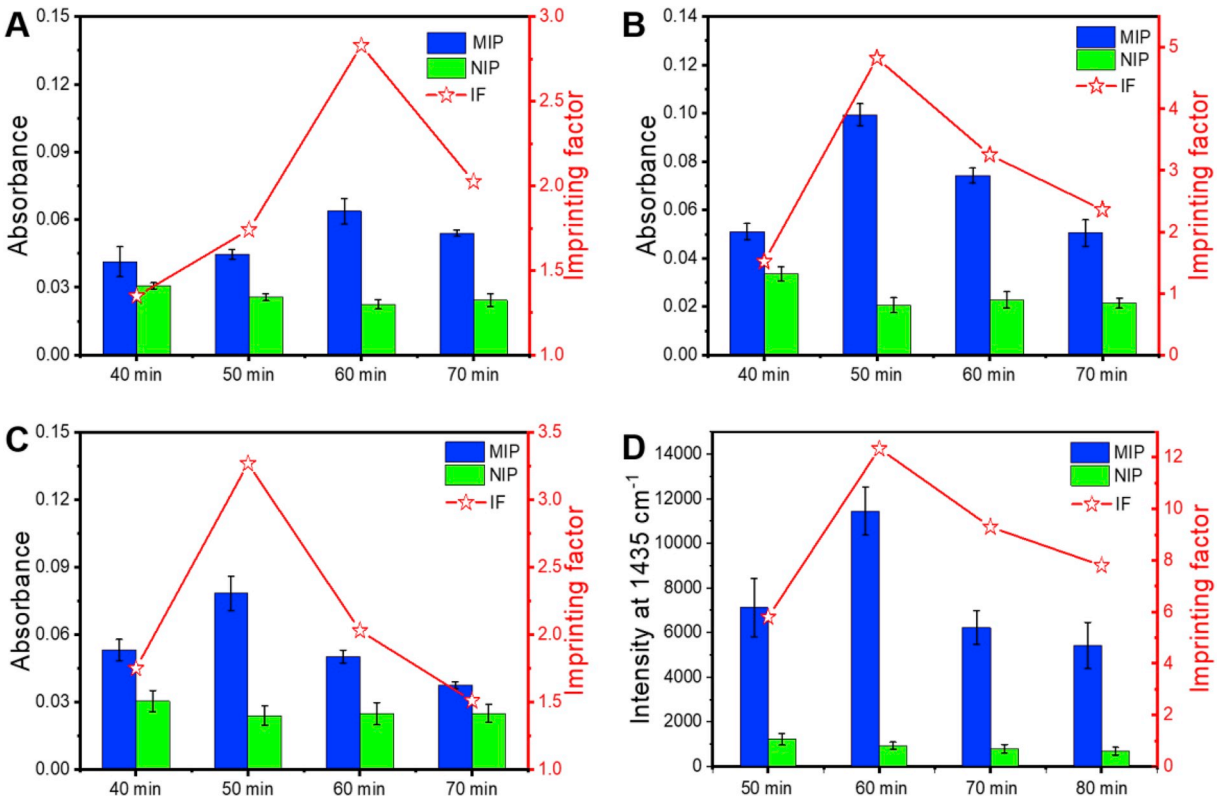

Fig. 1. Optimization of monomer ratio and imprinting time of epitope-imprinted arrays. Epitope-imprinted arrays and non-imprinted arrays prepared with the ratio of APTES/UPTES/IBTES/TEOS at (A) 10:10:20:60, (B) 15:15:30:40, and (C) 10:20:30:40 under different imprinting time; (D) Optimization of imprinting time of glycan-imprinted Ag/PATP@SiO_2 NPs. The error bars represent the standard deviation for three parallel experiments.

thickness of the imprinting layer was calculated to be 2.91 nm according to the thickness-imprinting time linear relationship previously established (Bie et al., 2015). Considering the glycans were immobilized via a formylphenylboronic acid (the length is ca. 0.6 nm), the template length coverage by the imprinting layer was calculated to be within 63%–127% (see Table S3). This means that while some short glycans were completely embedded within the imprinting layer, most of the glycans were well covered and thereby the prepared molecularly imprinted Raman nanotags should be able to bind most of the glycans. Although it is hard to experimentally confirm this estimation due to the lack of pure glycans of the target glycoprotein, such estimated template length coverage has been proved to be a useful guide for the imprinting of glycans and monosaccharides (Bie et al., 2015, 2018; Yin et al., 2015; Wang et al., 2016; Dong et al., 2019).

3.4. Optimization of extraction time and labeling time

In order to quickly and sensitively detect the target, the extraction time by the epitope-imprinted array and the labeling time by the glycan-imprinted Ag/PATP@SiO_2 NPs were optimized. As shown in Fig. S6A, the Raman intensity increased with the extraction time in 5–20 min, and remained almost unchanged with the further increase of the extraction time after 20 min. Thus, 20 min was chosen as the optimal extraction time for subsequent experiments. As shown in Fig. S6B, the Raman intensity increased with the increase of the labeling time in 2–5 min, and after 5 min, the Raman intensity remained almost unchanged as further increasing the labeling time. Thus, 5 min was considered the best labeling time and used for further experiments. Such short extraction time and labeling time facilitate rapid determination of the target.

3.5. Selectivity test

In order to investigate the selectivity of the epitope-imprinted arrays, the glycans-imprinted Raman nanotags and the developed PISA approach, the target CEA and five interfering proteins, including horseradish peroxidase (HRP, glycoprotein), bovine serum albumin (BSA, non-glycoprotein), human apo-transferrin (TRF, glycoprotein), ribonuclease B (RNase B, glycoprotein) and β-casein (non-glycoprotein), were used as test proteins. The selectivity of the epitope-imprinted arrays was evaluated by UV absorbance of the protein captured by the array. As shown in Fig. 2A, the cross-reactivity ranged from 7.2 to 14.4%, which was well acceptable. In order to examine the selectivity of the glycans-imprinted Ag/PATP@SiO_2 NPs, FPBA-modified arrays were used substrates to capture the test proteins, while the captured protein was labeled with glycan-imprinted Ag/PATP@SiO_2 NPs. As shown in Fig. 2B, even the concentrations of the interfering proteins were 100-fold higher than that of the target, the cross-reactivity was within 6.3–15.2%, indicating that the glycans-imprinted Raman nanotags exhibited good selectivity to the target protein. As a comparison, with using the epitope-imprinted arrays as well as the glycans-imprinted Raman nanotags, the developed odMIP-PISA approach exhibited apparently improved selectivity to the target protein. As shown in Fig. 2C, the cross-reactivity was reduced to 5.2–8.2%. The improved selectivity was mainly due to the double characteristic recognition strategy of the odMIP-PISA approach.

3.6. Binding isotherm and linear response curve

With the developed odMIP-PISA approach, binding isotherms for an epitope-imprinted assay and a non-imprinted array were investigated. As shown in Fig. 3, the imprinted array exhibited target concentration dependent response whereas the non-imprinted array exhibited nearly

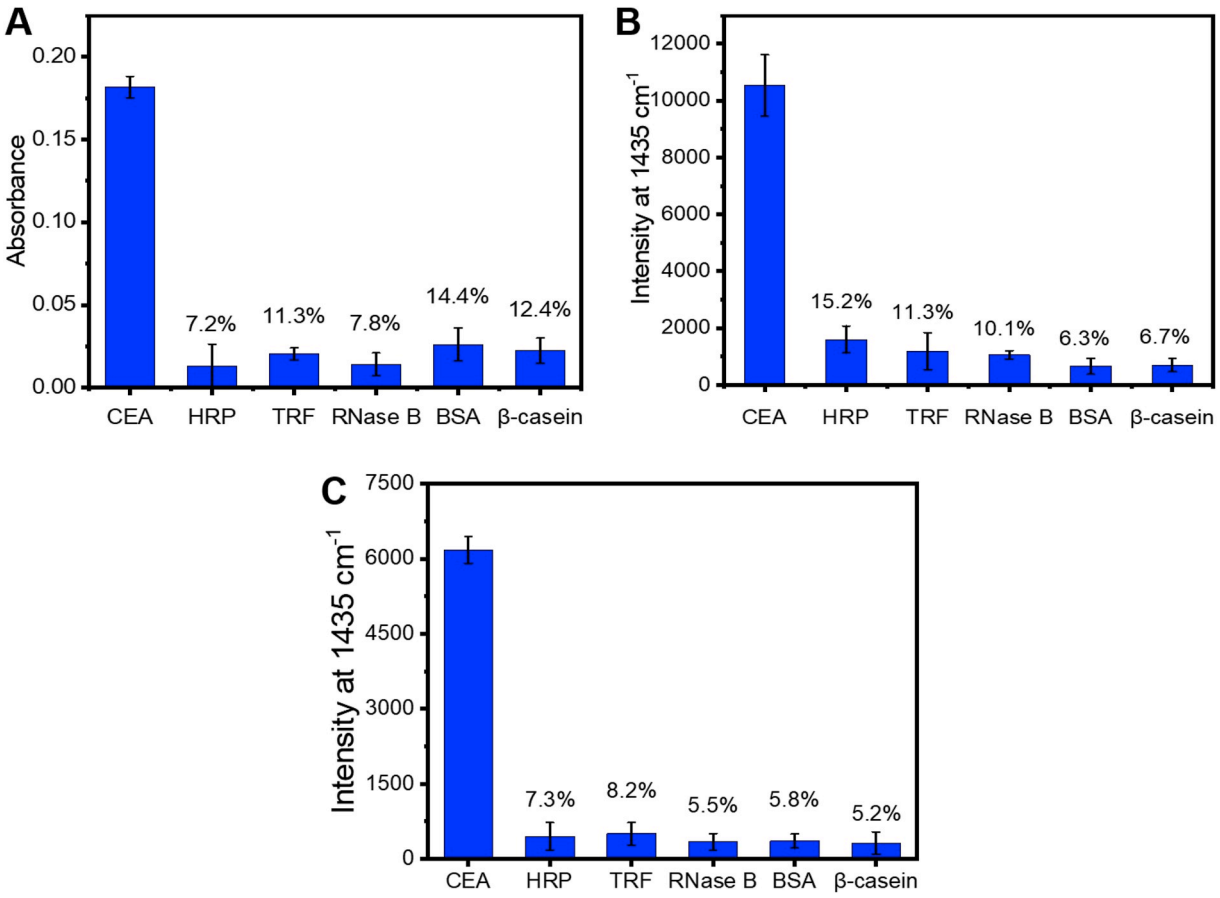

Fig. 2. Selectivity test. (A) UV absorbance for different proteins captured by epitope-imprinted arrays. (B) Raman intensity for different protein captured by glycan-imprinted Ag/PATP@SiO_2 NPs. (C) Raman intensity for different proteins detected the odMIP-PISA method. Samples: 1 mg/mL interfering protein or 0.01 mg/mL CEA dissolved in 10 mM phosphate buffer (pH 7.4). The error bars represent the standard deviation for three parallel experiments.

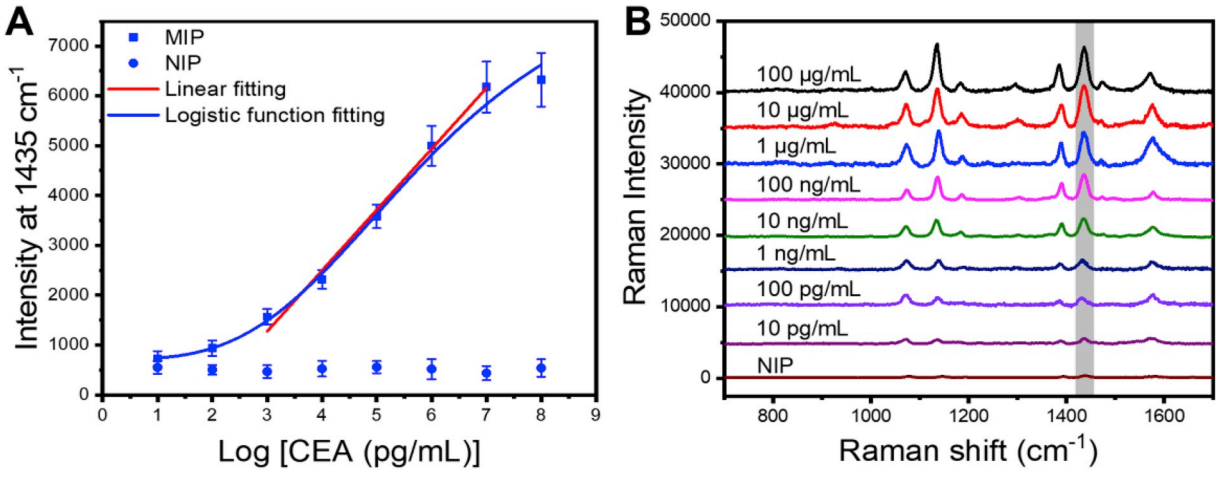

Fig. 3. (A) Concentration-dependent Raman response of odMIP-PISA approach and corresponding PISA with dual NIPs, and (B) Raman spectra for CEA at different concentrations detected by the odMIP-PISA and corresponding PISA with dual NIPs. The error bars represent the standard deviation for three parallel experiments.

no response. The Raman peak intensity at 1435 cm^{-1} gradually increased with increasing the concentration of CEA. Via fitting the intensity against the logarithm of CEA concentration, the K_d value for the epitope-imprinted array was estimated to be 5.6×10^{-9} M. On the other hand, it can be found that within the concentration range of 1 ng/mL – 10 μg/mL, the dependence of the intensity on the logarithm of concentration was linear ($y = 1220.37\ x$ - 2386.27, $R^2 = 0.991$). The limit of detection (LOD) and limit of quantity (LOQ) of the approach were measured to be 5.6×10^{-14} M (S/N = 10) and 5.6×10^{-12} M (S/N = 10), respectively. The LOD is comparable to the data previously reported (Tu et al., 2016) while the LOQ is comparable to the level previously reported (Li et al., 2019). In addition, the reproducibility of Raman signal intensity was examined (Fig. S7). The SERS spectra were read from 30 random points on the imprinted array at a concentration of 100 ng/mL, and the RSD% of Raman signal at 1435 cm^{-1} was found to be ca. 7%. Such excellent reproducibility benefited from to evenly distributed

AuNPs on the imprinted array (Figs. S5G and S5H).

3.7. Real-world application and comparison with commercial kit-based ELISA

Since the serum CEA level in healthy human is equal or lower than 5 ng/mL (Chen et al., 2014) while the CEA level in cancer patient serum is generally higher than 10 ng/mL (Ni et al., 2005), the developed odMIP-PISA approach is well suitable for the detection of serum CEA for early cancer screening. The serum CEA levels of a healthy individual and a colon cancer patient were measured with the developed odMIP-PISA approach. According to the linear calibration curve, the serum CEA levels were calculated to be 1.7 ± 0.5 ng/mL and 21.3 ± 6.7 ng/mL of the healthy individual and the cancer patient, respectively. These results are in good agreement with the previously reported results (Chen et al., 2014; Ni et al., 2005). In addition, these results relied on the assumption that the matrix effect could effectively eliminated by using the MIP-based extraction. To verify such assumption is reasonable, we further performed the improved standard addition method (Tu et al., 2016). The serum samples were spiked with a limited volume of standard CEA solution with known concentrations (c_i), and the spiked serum samples were measured by the odMIP-PISA. Since the initial concentrations (c_0) of the serum samples have been measured, the total CEA concentrations ($c_0 + c_i$) in the spiked serum samples can be calculated. Then, the Raman intensity at 1435 cm^{-1} was plotted against the logarithm of the total CEA concentrations of the spiked serum samples. If the obtained linear relationships exhibited a very good linearity, then it means that the assumption is acceptable and the initially obtained values can be considered as the test results. The Raman spectra and the intensity at 1435 cm^{-1} for the spiked serum samples from the healthy individual and the colon cancer patient are shown Fig. 4. As shown in Fig. S8, the intensity-log c relationships exhibited very good linearity. If a higher or lower c_0 value was taken for plotting, the linearity for the plot of the Raman signal intensity against the logarithm of the value of $c_0 + c_i$ became apparently worse, suggesting that the assumption of negligible matrix effect was reasonable. Thus, the initially measured results are considered as the final test results for the samples measured.

The CEA concentration in the serum of colon cancer patient was also quantified by ELISA based on a commercial kit and compared with the odMIP-PISA method. Fig. S9 shows the linear calibration curve of the ELISA; the OD value increased linearly with increasing the CEA concentration within the range from 1 ng/mL to 65 ng/mL. According to the linear calibration curve, the CEA concentration of the colon cancer patient and healthy individual were calculated respectively to be 17.3 ± 1.5 ng/mL and 1.5 ± 0.4 ng/mL, which are close to corresponding results by the current method. In order to robustly validate the odMIP-PISA method for clinical application, 10 more clinical serum samples were detected by commercial kit-based ELISA and this method. As shown in Table S4, the results by the current method are in good agreement with those by ELISA, indicating the reliability and feasibility of the current method for real sample application. However, as compared in Table 1, our method exhibited several advantages: 1) faster speed, 30 min as compared with 4.5 h by the ELISA; 2) simplified procedure, requiring only 6 steps totally, as compared with 32 steps by the ELISA; 3) less sample volume consumption, requiring only 5 μL, as compared with 50 μL by the ELISA); 4) More cost-efficient, be about 10

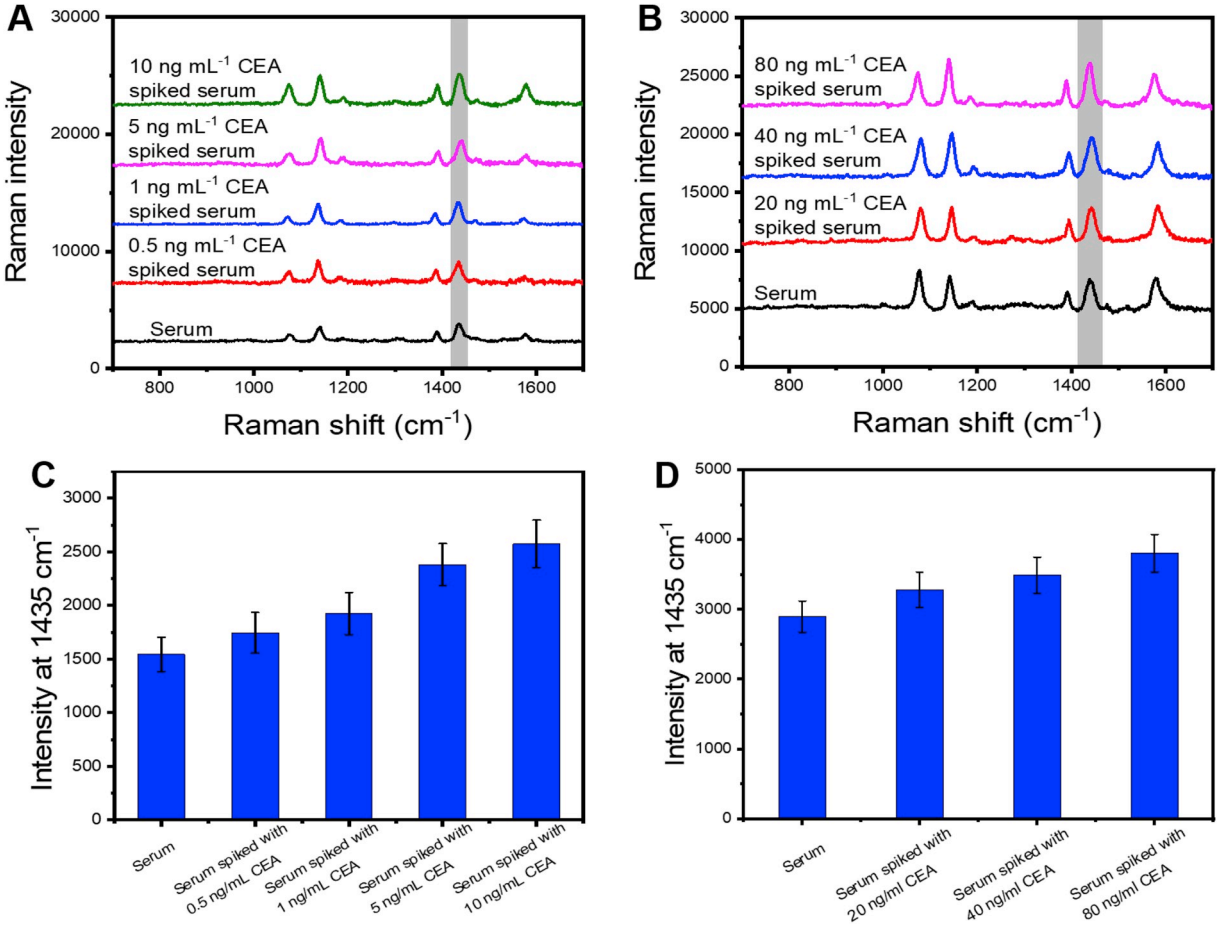

Fig. 4. Raman spectra for healthy individual (A) and colon cancer patient (B) serum samples unspiked and spiked with different concentrations of CEA; Raman intensities at 1435 cm^{-1} for healthy individual (C) and colon cancer patient (D) serum samples unspiked and spiked with different concentrations of CEA. The error bars represent the standard deviation for three parallel experiments.

Table 1
Comparison of the performance of commercial ELISA kit and odMIP-PISA.

Item	Commercial CEA ELISA kit	odMIP-PISA
Linear range	1 – 65 ng/mL	1 ng/mL – 10 μg/mL
Serum CEA concentration of healthy individual	1.5 ± 0.4 ng/mL	1.7 ± 0.5 ng/mL
Serum CEA concentration of colon cancer patient	17.3 ± 1.2 ng/mL	21.3 ± 6.7 ng/mL
Time required	4.5 h	30 min
Number of steps required	32	6
Sample volume required	50 μL	5 μL
Cost	¥ 51	¥ 5.8

*The values after the symbol "±" represent the standard deviation for three parallel experiments.

times cheaper in cost as compared with the ELISA. Besides, the odMIP-based approach has two strengths: 1) long term stability, which is a general intrinsic advantage of MIPs over antibodies; and 2) glycan specificity of the Raman nanotag, which is a unique merit of glycan-imprinted MIPs over antibodies because of the low immunogenicity of glycans.

4. Conclusion

In this study, we have developed a new strategy called odMIP-PISA for specific determination of glycoprotein disease biomarkers. To the best of our knowledge, this is the first report on the detection of a glycoprotein through simultaneously recognizing the peptide chain feature (epitope) as well as the glycosylation feature (glycans) by two different types of MIPs. Such orthogonal double recognition greatly ensured the detection specificity. Meanwhile, the plasmonic detection provided ultrasensitive detection. This odMIP-PISA approach permitted facile detection of the CEA concentration in serum samples, which allowed for differentiation of colon cancer patient from healthy individual. This method exhibited multiple advantages, such as speed, limited sample requirement, stability and cost efficiency. This approach can be extended to a large variety of glycoproteins, since the imprinting approaches involved are widely applicable. However, it should be noted that, if one or more amino acids on the epitope is modified with PTM, the imprinting of a post-translationally modified epitope is still challenging. Hopefully, such situation less frequently occurs. There are epitope options, i.e., C-terminal epitope and N-terminal epitope. Meanwhile, C-terminal epitopes are rarely post-translationally modified. As for future development, it is a promising direction to differentiate and quantitate specific glycans of a glycoprotein target using single glycan-specific MIPs. It is critically important for more specific diagnosis of particular cancers and differentiation of exogenous hormone (such as recombinant erythropoietin) from its native counterpart in antidoping analysis in sports. Therefore, this approach will hold great application prospects in multiple important areas, such as clinical diagnosis, biochemical research, and antidoping analysis.

Declaration of competing interest

The authors declare no competing interest.

CRediT authorship contribution statement

Lingli Zhou: Investigation, Validation, Writing - original draft. **Yijia Wang:** Investigation, Data curation, Writing - original draft. **Rongrong Xing:** Investigation. **Jin Chen:** Resources. **Jia Liu:** Resources. **Wei Li:** Investigation. **Zhen Liu:** Conceptualization, Supervision, Resources, Writing - review & editing.

Acknowledgements

We acknowledge the financial support from the National Natural Science Foundation of China (grant numbers: 21425520, 21627810 and 21834003).

Appendix A. Supplementary data

Supplementary data to this article can be found online at https://doi.org/10.1016/j.bios.2019.111729.

References

Adbo, K., Nicholls, I.A., 2001. Anal. Chim. Acta 435, 115–120.
Andersson, L., Sellergren, B., Mosbach, K., 1984. Tetrahedron Lett. 25, 5211–5214.
Awino, J.K., Zhao, Y., 2013. J. Am. Chem. Soc. 135, 12552–12555.
Baker, M., 2015. Nature 527, 545–551.
Baker, M., 2015. Nature 521, 274–276.
Bi, X.D., Liu, Z., 2014. Anal. Chem. 86, 959–966.
Bie, Z.J., Chen, Y., Ye, J., Wang, S.S., Liu, Z., 2015. Angew. Chem. Int. Ed. 54, 10211–10215.
Bie, Z.J., Xing, R.R., He, X.P., Ma, Y.Y., Chen, H.Y., Liu, Z., 2018. Anal. Chem. 90, 9845–9852.
Bigalke, B., Potz, O., Kremmer, E., Geisler, T., Seizer, P., Puntmann, V.O., Gawaz, M., 2011. Clin. Chem. 57, 898–904.
Casey, B.J., Kofinas, P., 2010. J. Biomed. Mater. Res. 87A, 359–363.
Chen, L.C., Zeng, X.T., Si, P., Chen, Y.M., Chi, Y.W., Kim, D.H., Chen, G.N., 2014. Anal. Chem. 86, 4188–4195.
Chianella, I., Guerreiro, A., Moczko, E., Caygill, J.S., Piletska, E.V., Perez De Vargas Sansalvador, I.M., Whitcombe, M.J., Piletsky, S.A., 2013. Anal. Chem. 85, 8462–8468.
Cho, C.H., Kim, J.H., Song, D., Park, T.J., Park, J.P., 2019. Biosens. Bioelectron. 142, 111482.
Choi, H.K., Shon, H.K., Yu, H., Lee, T.G., Kim, Z.H., 2013. J. Phys. Chem. Lett. 4, 1079–1086.
Clark, M.F., Adams, A.N., 1977. J. Gen. Virol. 34, 475–483.
Deshayes, S., Cabral, H., Ishii, T., Miura, Y., Kobayashi, S., Yamashita, T., Matsumoto, A., Miyahara, Y., Nishiyama, N., Kataoka, K., 2013. J. Am. Chem. Soc. 35, 15501–15507.
Diaz-Fernandez, A., Miranda-Castro, R., de-los-Santos-Álvarez, N., Rodríguez, E.F., Lobo-Castañón, M.J., 2019. Biosens. Bioelectron. 128, 83–90.
Dong, Y.R., Li, W., Gu, Z.K., Xing, R.R., Ma, Y.Y., Zhang, Q., Liu, Z., 2019. Angew. Chem., Int. Ed. Engl. 58, 10621–10625.
Engvall, E., Perlmann, P., 1971. Immunochemistry 8, 871–874.
Gervay, J., Mcreynolds, K.D., 1999. Curr. Med. Chem. 6, 129–153.
Haab, B.B., 2010. Expert Rev. Proteomics 7, 9–11.
Huang, C., Zhan, T., Liu, Y., Li, Q., Wu, H., Ji, D., Li, Y., 2015. Clin. Proteonomics 12, 17–23.
Huang, Y.F., Zhu, H.P., Liu, G.K., Wu, D.Y., Ren, B., Tian, Z.Q., 2010. J. Am. Chem. Soc. 132, 9244–9246.
Huang, Y.Z., Fang, Y.R., Yang, Z.L., Sun, M.T., 2010. J. Phys. Chem. C 114, 18263–18269.
Kammeijer, G.S.M., Nouta, J., de la Rosette, J.J.M.C.H., de Reijke, T.M., Wuhrer, M., 2018. Anal. Chem. 90, 4414–4421.
Kannicht, C., Lucka, L., Nuck, R., Reutter, W., Gohlke, M., 1999. Glycobiology 9, 897–906.
Kim, S., Lee, H.J., 2015. Anal. Chem. 87, 7235–7240.
Kimura, H., Matsuzawa, S., Tu, C.Y., Kitamori, T., Sawada, T., 1996. Anal. Chem. 68, 3063–3067.
Kubo, T., Nomachi, M., Nemoto, K., Sano, T., Hosoya, K., Tanaka, N., Kaya, K., 2006. Anal. Chim. Acta 577, 1–7.
Laboria, N., Fragoso, A., Kemmner, W., Latta, D., Nilsson, O., Luz Botero, M., Drese, K., O'Sullivan, C.K., 2010. Anal. Chem. 82, 1712–1719.
Lehle, L., Strahl, S., Tanner, W., 2006. Angew. Chem., Int. Ed. Engl. 45, 6802–6818.
Li, C., Wang, L.X., 2018. Chem. Rev. 118, 8359–8413.
Li, L., Lu, Y., Bie, Z.J., Chen, H.Y., Liu, Z., 2013. Angew. Chem. Int. Ed. 129, 2871-2871.
Li, Q.R., Yang, K.G., Liang, Y., Jiang, B., Liu, J.X., Zhang, L.H., Liang, Z., Zhang, Y.K., 2014. ACS Appl. Mater. Interfaces 6, 21954–21960.
Li, W., Zhang, Q., Wang, Y.J., Ma, Y.Y., Guo, Z.C., Liu, Z., 2019. Anal. Chem. 91, 4831–4837.
Liu, J., Yin, D.Y., Wang, S.S., Chen, H.Y., Liu, Z., 2016. Angew. Chem. Int. Ed. 55, 13215–13218.
Liu, J.Q., Wulff, G., 2004. J. Am. Chem. Soc. 126, 7452–7453.
Lucka, L., Fernando, M., Grunow, D., Kannicht, C., Horst, A.K., Nollau, P., Wagener, C., 2005. Glycobiology 15, 87–100.
Muhammad, P., Tu, X.Y., Liu, J., Wang, Y.J., Liu, Z., 2017. ACS Appl. Mater. Interfaces 9, 12082–12091.
Ni, X.G., Bai, X.F., Mao, Y.L., Shao, Y.F., Wu, J.X., Shan, Y., Wang, C.F., Wang, J., Tian, Y. T., Liu, Q., Xu, D.K., Zhao, P., 2005. Eur. J. Surg. Oncol. 31, 164–169.
Nishino, H., Huang, C.S., Shea, K.J., 2006. Angew. Chem. Int. Ed. 45, 2392–2396.
Qin, S.Y., Chen, N.D., Yang, X.H., Wang, Q., Wang, K.M., Huang, J., Liu, J.B., Zhou, M.G., 2017. ACS Sens. 2, 308–315.

Smolinska-Kempisty, K., Guerreiro, A., Canfarotta, F., Cáceres, C., Whitcombe, M.J., Piletsky, S.A., 2016. Sci. Rep. 6, 37638.
Sterner, E., Flanagan, N., Gildersleeve, J.C., 2016. ACS Chem. Biol. 11, 1773–1783.
Sun, X.L., Jian, Y.N., Wang, H., Ge, S.G., Yan, M., Yu, J.H., 2019. ACS Appl. Mater. Interfaces 11, 16198–16206.
Surugiu, I., Ye, L., Yilmaz, E., Dzgoev, A., Danielsson, B., Mosbacha, K., Haupt, K., 2000. Analyst 125, 13–16.
Tu, X.Y., Muhammad, P., Liu, J., Ma, Y.Y., Wang, S.S., Yin, D.Y., Liu, Z., 2016. Anal. Chem. 88, 12363–12370.
Usta, D.D., Salimi, K., Pinar, A., Coban, I., Tekinay, T., Tuncel, A., 2016. ACS Appl. Mater. Interfaces 8, 11934–11944.
Vlatakis, G., Andersson, L.I., Müller, R., Mosbach, K., 1993. Nature 361, 645–647.
Wang, S.S., Yin, D.Y., Wang, W.J., Shen, X.J., Zhu, J.J., Chen, H.Y., Liu, Z., 2016. Sci. Rep. 6, 22757.
Wang, X., Wang, L.Y., He, X.W., Zhang, Y.K., Chen, L.X., 2009. Talanta 78, 327–332.
Wulff, G., Sarhan, A., 1972. Angew. Chem., Int. Ed. Engl. 11, 341–345344.
Xing, R.R., Ma, Y.Y., Wang, Y.J., Wen, Y.R., Liu, Z., 2019. Chem. Sci. 10, 1831–1835.
Xing, R.R., Wang, S.S., Bie, Z.J., He, H., Liu, Z., 2017. Nat. Protoc. 12, 964–987.
Xu, J.J., Haupt, K., Bernadette, T.S.B., 2017. ACS Appl. Mater. Interfaces 9, 24476–24483.
Yazawa, S., Yokobori, T., Kaira, K., Kuwano, H., Asao, T., 2018. Clin. Chim. Acta 478, 120–128.
Yazdanparast, S., Benvidi, A., Banaei, M., Nikukar, H., Tezerjani, M.D., Azimzadeh, m., 2018. Microchim. Acta 185, 405.
Ye, J., Chen, Y., Liu, Z., 2014. Angew. Chem. Int. Ed. 126, 10554–10557.
Yin, D.Y., Wang, S.S., He, Y.J., Liu, J., Zhou, M., Ouyang, J., Liu, B.R., Chen, H.Y., Liu, Z., 2015. Chem. Commun. 51, 17696–17699.
You, M., Yang, S., Tang, W.X., Zhang, F., He, P.G., 2017. ACS Appl. Mater. Interfaces 9, 13855–13864.
Yue, T.T., Goldstein, I.J., Hollingsworth, M.A., Kaul, K., Brand, R.E., Haab, B.B., 2009. Mol. Cell. Proteom. 8, 1697–1707.
Zhou, Y.L., Zhang, H.Q., Liu, L.T., Li, C.M., Zhu, C., Zhu, X., Ye, B.X., Xu, M.T., 2016. Sci. Rep. 6, 35186.